

Head-Aware KV Cache Compression for Efficient Visual Autoregressive Modeling

Ziran Qin
qinziran@sjtu.edu.cn
School of Electronic Information and
Electrical Engineering, Shanghai Jiao
Tong University
Shanghai 200240, China

Youru Lv
mishall0914@sjtu.edu.cn
School of Electronic Information and
Electrical Engineering, Shanghai Jiao
Tong University
Shanghai 200240, China

Mingbao Lin*
linmb001@outlook.com
Skywork AI
Singapore 118222, Singapore

Zeren Zhang
eric_zhang@stu.pku.edu.cn
School of Mathematical Sciences,
Peking University
Beijing 100871, China

Danping Zou
dpzou@sjtu.edu.cn
School of Electronic Information and
Electrical Engineering, Shanghai Jiao
Tong University
Shanghai 200240, China

Weiyao Lin*
wylin@sjtu.edu.cn
School of Electronic Information and
Electrical Engineering, Shanghai Jiao
Tong University
Shanghai 200240, China

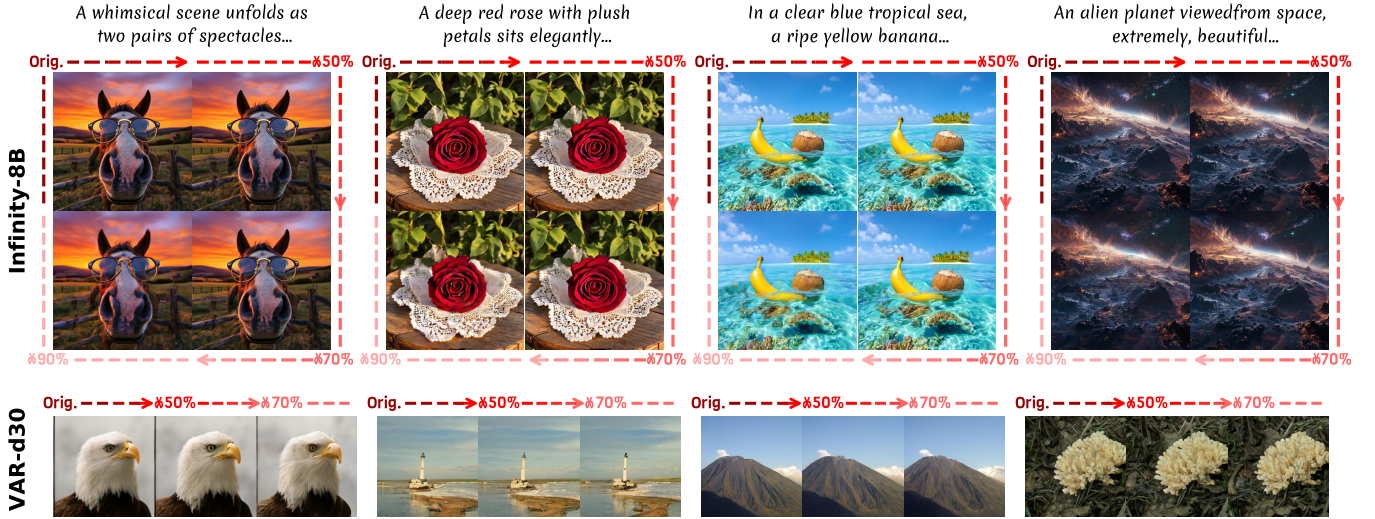


Figure 1: HACK effectively hacks down KV cache for Infinity and VAR models, maintaining high-quality generation while slashing memory usage by up to 58.9% and 44.2% respectively.

Abstract

Visual Autoregressive (VAR) models have emerged as a powerful approach for multi-modal content creation, offering high efficiency and quality across diverse multimedia applications. However, they face significant memory bottlenecks due to extensive KV cache accumulation during inference. Existing KV cache compression techniques for large language models are suboptimal for VAR models due to, as we identify in this paper, two distinct categories of attention heads in VAR models: *Structural Heads*, which preserve spatial coherence through diagonal attention patterns, and *Contextual Heads*, which maintain semantic consistency through vertical attention patterns. These differences render single-strategy KV compression techniques ineffective for VAR models. To address this, we propose HACK, a training-free **Head-Aware** Compression

method for KV cache. HACK allocates asymmetric cache budgets and employs pattern-specific compression strategies tailored to the essential characteristics of each head category. Experiments on Infinity-2B, Infinity-8B, and VAR-d30 demonstrate its effectiveness in text-to-image and class-conditional generation tasks. HACK can hack down up to 50% and 70% of cache with minimal performance degradation for VAR-d30 and Infinity-8B, respectively. Even with 70% and 90% KV cache compression in VAR-d30 and Infinity-8B, HACK still maintains high-quality generation while reducing memory usage by 44.2% and 58.9%, respectively.

1 Introduction

Autoregressive (AR) models [1, 2, 10, 26] have achieved great success in text generation. However, traditional AR models [19, 24, 36] have struggled with image generation, where diffusion models [4, 11, 21, 31, 32] outperform them by using a continuous denoising

*Corresponding author.

process to produce high-quality images efficiently. The emergence of visual autoregressive modeling (VAR) [37] has well improved AR models' generation efficiency. By adopting a multi-scale, coarse-to-fine prediction strategy, VAR enables parallel generation of multiple tokens, greatly reducing inference steps. As a result, VAR generates high-quality images in seconds, surpassing the diffusion models.

However, VAR models still face memory bottlenecks during inference due to KV cache accumulation. The progressive multi-scale strategy requires storing KV states from all previous tokens—often exceeding the memory demands of traditional AR models—making this issue especially severe for high-resolution images. For example, generating 1024×1024 images with a batch size of 8 using Infinity-8B [18], a VAR-based text-to-image model, requires processing over 10K tokens across multiple scales, with KV caching alone consuming approximately 90 GB of memory. This poses a major challenge for practical deployment. Recent advances in KV cache compression [25, 33, 41, 47] for large language models (LLMs) and vision-language models (VLMs) offer promising strategies to reduce memory usage in AR models. However, applying these methods directly to VAR models is difficult due to fundamental differences in their attention mechanisms.

As shown in Figure 2(a,b), attention patterns in LLMs and VLMs are mostly vertical, focusing on initial, recent, and special tokens. This sparsity enables aggressive pruning without significant loss of fidelity. In contrast, VAR (Figure 2(c)) features attention heads with diagonal or band-like patterns, attending mainly to spatially adjacent tokens, regardless of semantics. These **Structural Heads** play a crucial role in preserving geometric coherence, ensuring that the spatial integrity of generated images retains intact. Conversely, another class of heads demonstrates vertical attention patterns akin to those observed in LLMs and VLMs, selectively attending to key tokens independent of spatial positioning to maintain thematic and semantic consistency. We designate these as **Contextual Heads**. Given these intrinsic distinctions, existing KV cache compression techniques, which are predominantly optimized for vertical attention patterns, prove suboptimal when applied to VAR models. These methods fail to accommodate the dual nature of attention mechanisms in VAR models, particularly the structural dependencies that are essential for high-quality image generation. Therefore, advancing KV cache compression for VAR models necessitates novel approaches that account for both structural and contextual attention heads, ensuring a balanced trade-off between memory efficiency and generative fidelity.

To tackle the challenges of efficient KV cache management in VAR models, we propose **HACK**, a novel, training-free head-aware compression framework. HACK leverages the inherent differences between structural and contextual attention heads by introducing a robust offline classification strategy for precise head categorization based on attention patterns. This is followed by an asymmetric cache budget allocation mechanism, applying more aggressive compression to contextual heads due to their sparsity and robustness while preserving positional information in structural heads. HACK also incorporates pattern-specific compression strategies tailored to the unique characteristics of each head type. Extensive experiments on state-of-the-art VAR architectures, including Infinity-2B, Infinity-8B, and VAR-d30, show the superior performance of HACK. Specifically, HACK achieves significant KV cache compression of

up to 50% in VAR-d30 and 70% in Infinity-8B with negligible performance loss. Remarkably, even at more aggressive compression levels (70% for VAR-d30 and 90% for Infinity-8B), HACK continues to deliver high-quality generation outputs while reducing memory consumption by 44.2% and 58.9%, respectively. To the best of our knowledge, HACK is the first framework specifically addressing KV cache compression in VAR models.

Our key contributions made in this paper are:

- We conduct an in-depth analysis, identify and characterize structural and contextual attention heads, providing insights crucial for effective KV cache compression.
- We introduce HACK, a head-aware, training-free framework for VAR models, featuring asymmetric cache budget allocation and optimized KV cache compression strategies.
- We validate HACK on multiple VAR models, demonstrating substantial improvements in memory efficiency while preserving or enhancing generation quality.

2 Related Work

Autoregressive Visual Generation. AR models [1, 2, 10, 26], originally successful in LLMs, have extended into the visual domain, driving advancements in image generation. Traditional visual AR approaches [19, 24, 36] rely on next-token prediction, where images are first quantized into discrete tokens (e.g., VQVAE [38], VQGAN [12]) and then decoded autoregressively. While effective, these methods suffer from high computational costs and quantization inaccuracies, limiting their efficiency compared to diffusion models. Recently, VAR models [3, 18, 34, 37] have introduced a next-scale prediction paradigm, leveraging hierarchical parallel decoding for multi-scale image generation in fewer inference steps, improving both generation quality and speed, and making VAR models widely applicable in tasks such as text-to-image synthesis [18, 39], 3D content creation [5, 15], and unified visual understanding [48]. VAR models suffer from heavy KV cache accumulation during inference. To tackle this, we propose efficient, VAR-specific KV cache compression to reduce memory usage while preserving visual quality.

KV Cache Compression. Existing methods primarily focus on quantization, eviction, and merging strategies to mitigate KV cache memory overhead in LLMs and VLMs. Quantization [20, 23, 29, 45] reduces cache size by lowering bit precision but offers limited compression due to granularity constraints. Eviction methods selectively discard less critical tokens based on attention metrics [25, 28, 30, 35, 47], optimizing cache allocation under fixed budgets [13, 14, 16, 33, 44]. Merging strategies [27, 40, 41, 46] further alleviate memory constraints by combining redundant KV pairs while preserving context. However, these methods fall short of VAR models, whose hierarchical attention demands careful preservation of structural and contextual dependencies. To address this, we propose specialized KV cache optimization techniques for VAR's unique attention patterns, achieving significant memory reduction without compromising generation quality.

3 Analysis on VAR

3.1 Preliminaries

Visual AutoRegressive Modeling. VAR extends autoregressive modeling from "next-token" to "next-scale" prediction. Given an

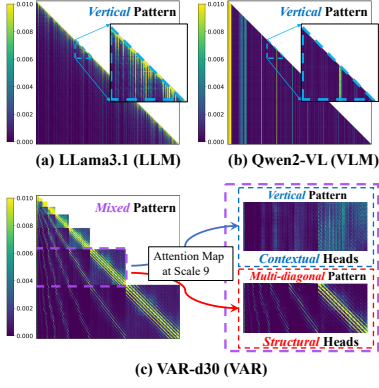


Figure 2: Attention patterns in LLM (a), VLM (b), and VAR (c). VAR shows mixed vertical and diagonal structures, unlike the vertical-only patterns in LLMs and VLMs.

image feature map $\mathbf{f} \in \mathbb{R}^{h \times w \times c}$, VAR quantizes it into K -scale token maps $\mathbf{R} = (\mathbf{r}_1, \mathbf{r}_2, \dots, \mathbf{r}_K)$, with the final map \mathbf{r}_K matching the original resolution. The probability distribution is:

$$p(\mathbf{r}_1, \mathbf{r}_2, \dots, \mathbf{r}_K) = \prod_{k=1}^K p(\mathbf{r}_k | \mathbf{r}_1, \mathbf{r}_2, \dots, \mathbf{r}_{k-1}), \quad (1)$$

where each $\mathbf{r}_k \in [V]^{h_k \times w_k}$ contains $h_k \times w_k$ tokens, and preceding scales provide context for generating \mathbf{r}_k . VAR generates all tokens for each scale in parallel, balancing efficiency and quality.

KV Cache in VAR. Akin to AR, VAR improves efficiency by storing KV states across multiple generation steps. In a multi-head attention module with H heads, each head $h \in \{1, \dots, H\}$ has its own weight matrices $\mathbf{W}_Q^{(h)}, \mathbf{W}_K^{(h)}, \mathbf{W}_V^{(h)} \in \mathbb{R}^{D \times D_h}$, projecting input tokens $\mathbf{X}_k \in \mathbb{R}^{T_k \times D}$ at step k into queries, keys, and values:

$$\mathbf{Q}_k^{(h)} = \mathbf{X}_k \mathbf{W}_Q^{(h)}, \quad \mathbf{K}_k^{(h)} = \mathbf{X}_k \mathbf{W}_K^{(h)}, \quad \mathbf{V}_k^{(h)} = \mathbf{X}_k \mathbf{W}_V^{(h)}, \quad (2)$$

where $T_k = w_k h_k$ denotes the number of tokens at scale k . The KV caches are updated independently per head:

$$\mathbf{K}^{(h)} = \text{Concat}(\mathbf{K}^{(h)}, \mathbf{K}_k^{(h)}), \quad \mathbf{V}^{(h)} = \text{Concat}(\mathbf{V}^{(h)}, \mathbf{V}_k^{(h)}), \quad (3)$$

with KV caches' length T growing cumulatively from $\sum_{i=1}^{k-1} w_i h_i$ to $\sum_{i=1}^k w_i h_i$. The caches facilitate per-head attention computation:

$$\mathbf{O}^{(h)} = \text{Attn}(\mathbf{Q}^{(h)}, \mathbf{K}^{(h)}, \mathbf{V}^{(h)}). \quad (4)$$

Finally, all outputs are concatenated to form the final output:

$$\mathbf{O} = \text{Concat}(\mathbf{O}^{(1)}, \mathbf{O}^{(2)}, \dots, \mathbf{O}^{(H)}). \quad (5)$$

KV cache reduces computation but increases memory with token accumulation, making efficient management vital.

KV Cache Compression. An effective strategy for managing the KV cache is to constrain its size through compression techniques. We define the total cache budget $B_{\text{total}} = T_{\text{total}} \cdot H \cdot L$, which often exceeds the memory capacity of many devices during

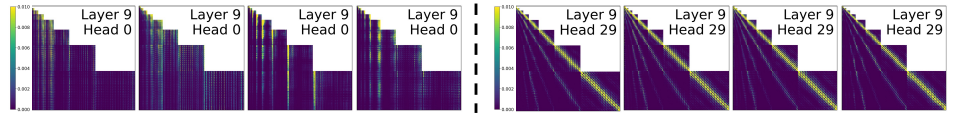


Figure 3: Attention maps of structural and contextual heads in VAR across scales and inputs. Both maintain consistent patterns. See supplementary for details.

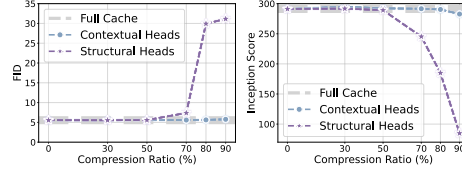


Figure 4: Compression robustness comparison between structural and contextual heads. Structural heads are more sensitive to KV cache compression.

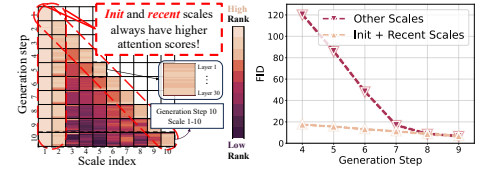


Figure 5: Scale-wise importance in VAR. (Left) Initial and recent scales get higher attention. (Right) Preserving them improves generation quality.

peak utilization. Here, $T_{\text{total}} = \sum_{i=1}^K w_i h_i$ represents the total number of tokens required for generation and L is the total number of layers. KV cache compression enables efficient memory management by maintaining the cache size within a fixed limit.

With a per-head budget B , once the cache length T exceeds B at any generation step, a compression function f is applied:

$$\hat{\mathbf{K}}^{(h)}, \hat{\mathbf{V}}^{(h)} = f(\mathbf{K}^{(h)}, \mathbf{V}^{(h)}, B), \quad (6)$$

where $\hat{\mathbf{K}}^{(h)}, \hat{\mathbf{V}}^{(h)} \in \mathbb{R}^{B \times D_h}$ denote the compressed KV cache for head h , constrained by budget B , ensuring efficient memory use while retaining key attention information.

3.2 In-depth Analysis of Attention Heads

We analyze the functional roles of attention heads using a VAR-d30 model for 256×256 image generation. Evaluations on 8K ImageNet samples are summarized in three parts:

Stability of Attention Heads across Inputs and Scales. We investigate whether attention types remain stable across varying image inputs and scales. By visualizing the attention weight maps of all heads at different generation steps and scales in VAR, using diverse input samples, we observe that each attention head consistently maintains its functional type—structural or contextual. In Figure 3, this stability is not in the exact shapes of the attention maps but in their overall patterns and focus. This invariance suggests that head behavior is primarily driven by internal role assignment rather than external factors like input content or resolution.

Compression Sensitivity of Different Heads. We hypothesize that contextual heads, with their concentrated vertical attention, are more resilient to compression than structural heads, which have spatially distributed attention. In Figure 4, contextual heads maintain high image quality even with up to 90% KV cache compression, while structural heads degrade significantly when compression exceeds 50%. These results suggest that excessive compression of structural heads disrupts critical spatial information, whereas contextual heads can tolerate higher compression with minimal quality

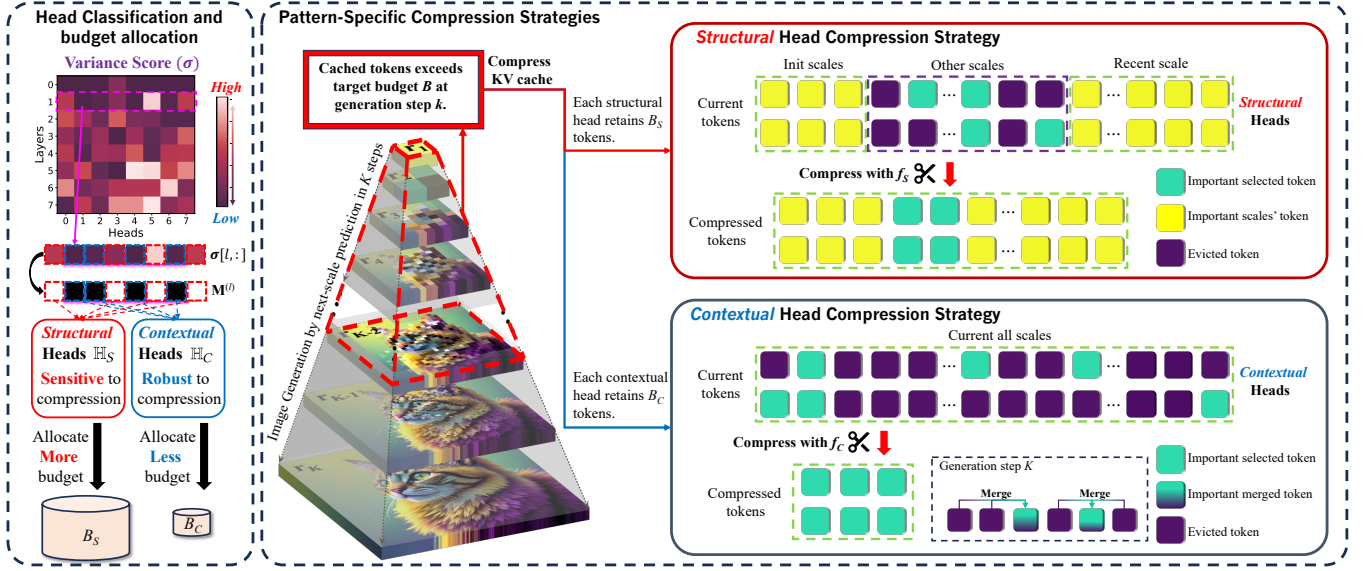


Figure 6: Overall framework of our proposed HACK method.

loss. This underscores the need for head-aware compression strategies that balance memory efficiency with generation fidelity.

Role of Initial and Recent Scales. In VAR’s generation, we find that not all scales contribute equally to overall quality. In Figure 5(Left), attention rankings reveal that the first two scales and the most recent scale consistently receive higher attention. Further, we compare two strategies: (1) preserving tokens from the initial two scales and the most recent scale, and (2) preserving tokens from intermediate scales. As shown in Figure 5(Right), strategy (1) yields much better generation quality, with FID scores up to $10\times$ lower than strategy (2) in early generation steps. This confirms the disproportionate importance of tokens from the initial and most recent scales in VAR’s generation process.

4 Methodology

4.1 Overall Framework

Based on our analysis, attention heads in VAR models exhibit two distinct and stable patterns: structural heads and contextual heads. For each layer, we define the sets of structural and contextual head indices as \mathbb{H}_S and \mathbb{H}_C , respectively, where $\mathbb{H}_S \cup \mathbb{H}_C = 1, \dots, H$ and $\mathbb{H}_S \cap \mathbb{H}_C = \emptyset$. This classification is derived through offline analysis (Section 4.2), as discussed later. To maintain clarity, we introduce superscript notations (C) and (S) to distinguish variables for contextual and structural heads, respectively. For example, $\mathbf{K}^{(C)}$, $\mathbf{V}^{(C)}$ denote the key and value states for contextual heads, while $\mathbf{K}^{(S)}$ and $\mathbf{V}^{(S)}$ represent those for structural heads.

Based on our finding that contextual and structural heads have markedly different sensitivities to compression, we adopt an asymmetric cache budget allocation strategy. Given an average target budget B per head and the proportion of contextual heads $0 < \alpha < 1$, we allocate budgets for contextual and structural heads as follows:

$$B_C = \lambda \cdot B, \quad B_S = \frac{(1 - \lambda)B}{1 - \alpha}, \quad (7)$$

where B_C and B_S denote the budgets allocated to each contextual and structural head, respectively. This allocation satisfies the total budget constraint $B = \alpha B_C + (1 - \alpha)B_S$, keeping overall memory usage constant. The hyperparameter λ controls the allocation asymmetry: smaller values assign less budget to contextual heads while reserving more capacity for spatially sensitive structural heads.

When the KV cache size for either head type surpasses its assigned budget, we apply compression strategies tailored to each head category. Specifically, for $p \in \{C, S\}$:

$$\hat{\mathbf{K}}^{(p)}, \hat{\mathbf{V}}^{(p)} = f_p(\{\mathbf{K}^{(h)} | h \in \mathbb{H}_p\}, \{\mathbf{V}^{(h)} | h \in \mathbb{H}_p\}, B_p), \quad (8)$$

where $f_p \in \{f_C, f_S\}$ denotes dedicated compression algorithms designed specifically for contextual and structural heads, respectively (detailed in Section 4.3). After compression, attention computation is performed separately for each head type, and the outputs are concatenated to reconstruct the final result, maintaining the original head order. Figure 6 illustrates our framework.

4.2 Offline Classification of Attention Head Patterns

Given the distinct attention patterns exhibited by contextual and structural heads, we introduce a direct yet productive offline classification method to distinguish these heads prior to model deployment. Contextual heads focus on specific tokens to capture semantic relationships, while structural heads demonstrate position-dependent shifting patterns to preserve spatial coherence.

To capture these differences, we analyze attention patterns at the final generation step K , as this step integrates interactions across all scales, providing the most comprehensive view of each head’s behavior throughout the entire generation process. Let $\mathbf{A}_K^{(l,h)} \in \mathbb{R}^{T_K \times T_{\text{total}}}$ denote the attention weights at step K for head h in layer l , where T_K represents the number of query tokens at the final scale. The fundamental distinction between the two head types can be

effectively captured by attention variance, formulated as:

$$\sigma_{l,h} = \sum_{j=1}^{T_{total}} \text{Var}(\mathbf{A}_K^{(l,h)}[:, j]). \quad (9)$$

We compute the column-wise variance across queries and sum the values to measure each head’s attention dependence on spatial structure versus semantic content. Structural heads show higher variance due to their position-aware attention, while contextual heads have lower variance, indicating a more uniform attention distribution across queries.

Prior to model deployment, we randomly sample N_s labels (for class-conditional image generation) or prompts (for text-to-image generation), depending on the model type. We then calculate the attention variance for each head across all layers, yielding an averaged variance score matrix $\sigma \in \mathbb{R}^{L \times H}$:

$$\sigma[l, h] = \frac{1}{N_s} \sum_{i=1}^{N_s} \sigma_{l,h}^{(i)}, \quad (10)$$

where $\sigma_{l,h}^{(i)}$ is i -th sample’s attention variance for head h in layer l .

Based on σ , we classify attention heads as contextual or structural by applying a threshold τ to the variance scores. For each layer l , we compute a binary classification mask $\mathbf{M}^{(l)} \in \{0, 1\}^H$:

$$\mathbf{M}^{(l)}[h] = \begin{cases} 0 & \text{if } \sigma[l, h] < \tau, \\ 1 & \text{otherwise.} \end{cases} \quad (11)$$

The threshold τ determines the global proportion α of contextual heads, which governs the asymmetric budget allocation between contextual and structural heads. Although applied globally, τ induces a layer-adaptive compression effect, as each layer allocates cache differently based on its specific head composition.

4.3 Pattern-Specific Compression Strategies

Leveraging attention scores to assess the importance of KV pairs is common in LLMs and VLMs. We extend this approach to VAR models, with key modifications to account for their unique structural and contextual characteristics. Existing KV cache eviction methods [25, 33] in language models rely on local attention scores within a limited window, optimizing computational efficiency and compatibility with frameworks like FlashAttention [8]. However, these methods miss global positional dependencies, which are crucial for VAR models, especially for structural heads.

To address this limitation, we introduce a query-subset attention computation approach. For a given head type $p \in \{S, C\}$, we uniformly sample a subset of query vectors $\tilde{\mathbf{Q}}_k^{(p)} \in \mathbb{R}^{N \times D_h}$ and compute attention scores against the full key matrix $\mathbf{K}^{(p)} \in \mathbb{R}^{L \times D_h}$, yielding an approximate attention matrix:

$$\tilde{\mathbf{A}}_k^{(p)} = \text{softmax}(\tilde{\mathbf{Q}}_k^{(p)} (\mathbf{K}^{(p)})^T). \quad (12)$$

Structural Head Compression Strategy f_S . Structural heads are sensitive to spatial structures and positional dependencies. Excessive compression can cause great loss of positional information, degrading generation quality. To solve it, we prioritize retaining critical positional information from the initial and recent scales.

When the KV cache for structural heads exceeds the allocated token budget B_S at generation step k , we apply the compression algorithm f_S . This ensures that L_{init} tokens from the initial scales and L_k tokens from the most recent scale are preserved. For intermediate-scale tokens, we select the most important KV pairs:

$$\mathbf{I}^{(S)} = \text{TOPK} \left(\sum_{i=1}^N \tilde{\mathbf{A}}_k^{(S)}[i, :], M \right), \quad M = B_S - L_{\text{init}} - L_k, \quad (13)$$

where TOPK selects the indices of the top- M tokens based on their cumulative attention scores. The compressed caches $\hat{\mathbf{K}}^{(S)}, \hat{\mathbf{V}}^{(S)}$ are:

$$\begin{aligned} \hat{\mathbf{K}}^{(S)} &= \text{Concat} \left(\mathbf{K}^{(S)}[:, L_{\text{init}}:], \mathbf{K}^{(S)}[\mathbf{I}^{(S)}, :], \mathbf{K}^{(S)}[-L_k : :] \right), \\ \hat{\mathbf{V}}^{(S)} &= \text{Concat} \left(\mathbf{V}^{(S)}[:, L_{\text{init}}:], \mathbf{V}^{(S)}[\mathbf{I}^{(S)}, :], \mathbf{V}^{(S)}[-L_k : :] \right). \end{aligned} \quad (14)$$

This strategy preserves critical global positional information while adhering to token budget constraints and remaining compatible with efficient attention computation frameworks.

Contextual Head Compression Strategy f_C . Contextual heads are more sparse in their attention distributions, allowing for aggressive compression without losing functionality. Unlike structural heads, which have position- and scale-dependent attention patterns, contextual heads focus on a small set of tokens and maintain stable attention across generation steps. When the KV cache for contextual heads exceeds the token budget B_C at generation step k , we identify the most critical KV pairs as follows:

$$\mathbf{I}^{(C)} = \text{TOPK} \left(\sum_{i=1}^N \tilde{\mathbf{A}}_k^{(C)}[i, :], B_C \right), \quad (15)$$

$$\mathbf{K}_{\text{sel}}^{(C)} = \mathbf{K}^{(C)}[\mathbf{I}^{(C)}, :], \quad \mathbf{V}_{\text{sel}}^{(C)} = \mathbf{V}^{(C)}[\mathbf{I}^{(C)}, :]. \quad (16)$$

where $\mathbf{I}^{(C)}$ denotes the indices of selected key tokens, while $\mathbf{K}_{\text{sel}}^{(C)}$ and $\mathbf{V}_{\text{sel}}^{(C)}$ are the corresponding key and value matrices.

Given the similarity between contextual head patterns and those in LLMs/VLMs, we apply KV cache merging techniques inspired by LOOK-M [41] to preserve contextual information integrity despite aggressive token reduction. Let $\mathbf{K}_{\text{dis}}^{(C)}$ and $\mathbf{V}_{\text{dis}}^{(C)}$ represent the KV pairs discarded during the importance-based selection. We integrate these discarded KV pairs with the selected ones ($\mathbf{K}_{\text{sel}}^{(C)}, \mathbf{V}_{\text{sel}}^{(C)}$) through many-to-one nearest-neighbor matching [7]. For each discarded token $\mathbf{k}_i \in \mathbf{K}_{\text{dis}}^{(C)}$, we identify its closest selected token $\mathbf{k}_j \in \mathbf{K}_{\text{sel}}^{(C)}$ by maximizing their similarity:

$$j = \arg \max_{j \in \mathbf{I}^{(C)}} u_{i,j}, \quad u_{i,j} = \mathbf{k}_i^T \mathbf{k}_j \quad (17)$$

For each selected key \mathbf{k}_j , we identify its most relevant discarded key \mathbf{k}_i (where $i \in \mathbb{N}_j$ and $\mathbf{k}_i \in \mathbf{K}_{\text{dis}}^{(C)}$) and apply a weighted merging strategy.

$$\mathbf{k}_j = \frac{1}{|\mathbb{N}_j| + 1} \left(\mathbf{k}_j + \sum_{i \in \mathbb{N}_j} u_{i,j} \cdot \mathbf{k}_i \right). \quad (18)$$

Here, $u_{i,j}$ is the weight for each discarded key \mathbf{k}_i , ensuring balanced integration between selected and discarded tokens. Following the alignment of KV pairs, we apply the same merging strategy to

Table 1: Quantitative comparison of text-to-image generation on Infinity-2B and Infinity-8B across two different compression ratios ρ . Evaluation is conducted using GenEval, DPG, HPSv2.1, and ImageReward (IR) metrics.

Method	$\rho(\%)$	GenEval \uparrow				DPG \uparrow				HPSv2.1 \uparrow	IR \uparrow
		Two Obj.	Position	Color Attri.	Overall	Entity	Relation	Attribute	Overall		
Infinity-2B											
Full	0%	0.79	0.27	0.61	0.68	88.98	92.42	86.49	82.68	30.49	0.946
H2O [47]	50%	0.78	0.27	0.60	0.69	89.11	92.34	86.19	82.74	30.30	0.936
SnapKV [25]	50%	0.77	0.28	0.62	0.69	89.00	93.08	86.13	82.71	30.22	0.933
LOOK-M [41]	50%	0.76	0.28	0.60	0.68	89.19	93.00	86.39	82.70	30.03	0.924
HACK	50%	0.79	0.28	0.57	0.69	89.08	92.65	86.15	82.84	30.51	0.942
H2O [47]	90%	0.60	0.17	0.31	0.54	87.25	92.26	82.43	79.50	24.40	0.501
SnapKV [25]	90%	0.58	0.20	0.32	0.53	86.95	92.84	82.81	79.61	24.31	0.544
LOOK-M [41]	90%	0.36	0.10	0.18	0.40	84.09	91.80	78.88	75.11	22.17	0.247
HACK	90%	0.74	0.27	0.55	0.66	89.42	93.46	85.97	83.21	28.59	0.862
Infinity-8B											
Full	0%	0.97	0.58	0.73	0.81	91.28	92.42	89.16	86.02	30.99	1.049
H2O [47]	50%	0.97	0.58	0.73	0.82	91.29	94.66	89.36	86.04	30.85	1.042
SnapKV [25]	50%	0.96	0.56	0.72	0.81	91.34	94.43	89.32	86.08	30.77	1.042
LOOK-M [41]	50%	0.96	0.58	0.72	0.82	91.29	94.35	89.46	86.16	30.67	1.034
HACK	50%	0.97	0.57	0.75	0.82	91.39	94.39	89.32	86.25	30.88	1.045
H2O [47]	90%	0.88	0.49	0.62	0.75	90.95	94.47	88.05	85.60	28.02	0.849
SnapKV [25]	90%	0.86	0.48	0.58	0.72	90.73	94.27	87.29	84.71	27.34	0.823
LOOK-M [41]	90%	0.75	0.43	0.48	0.66	90.26	94.43	86.55	84.17	26.99	0.747
HACK	90%	0.93	0.56	0.68	0.79	90.89	94.39	88.74	85.74	29.06	0.925

the value tokens. To avoid error propagation from early scales, we restrict the merging operation to the final generation step K .

5 Experimentation

5.1 Experiment Settings

Evaluation Models, Benchmarks and Metrics. We test three VAR models: Infinity-2B and Infinity-8B [18] for text-to-image generation, and VAR-d30 [37] for class-conditional generation. We evaluate different compression ratios ($\rho = 1 - \frac{B}{L_{\text{total}}}$). Metrics include GenEval [17], DPG [22], ImageReward [43], HPSv2.1 [42] for Infinity models, and FID-50k, sFID, Inception Score, Precision, and Recall for VAR, using 50 ImageNet1K [9] images per class at 256×256 resolution.

Baseline Methods. (1) Eviction-based methods: H2O [47], using accumulative attention scores, and SnapKV [25], based on clustered recent attention patterns; (2) Merging-based method: LOOK-M [41], merging evicted KV pairs following H2O’s strategy.

Implementation Details. We follow the original settings of Infinity and VAR for image generation. Additional implementation details for HACK are provided in the supplementary material.

5.2 Text-to-Image Generation

We first evaluate HACK alongside three baselines under varying compression ratios on Infinity-2B and Infinity-8B.

Quantitative Results. Table 1 presents results under memory-sufficient ($\rho = 50\%$) and memory-constrained ($\rho = 90\%$) settings. At $\rho = 50\%$, HACK outperforms all baselines, particularly on ImageReward and HPSv2.1, even surpassing the full KV cache in some cases. At $\rho = 90\%$, the performance gap widens significantly: while baseline methods degrade sharply, HACK maintains strong performance across all metrics. This robustness stems from its optimal budget allocation and compression strategy, which preserves critical information for spatial fidelity and compositional integrity.

Qualitative Results. Figure 7 shows HACK’s qualitative results at varying compression ratios on Infinity-2B/8B. As ρ increases from 50% to 90%, HACK consistently preserves scene layout, object structure, and semantic alignment with the original outputs. Even at extreme compression (e.g., $\rho = 90\%$), the images remain visually faithful, demonstrating HACK’s robustness. For more qualitative results, please refer to supplementary material.

Influence of Compression Ratios. Figure 8 plots ImageReward and HPSv2.1 across compression ratios. Baselines like H2O and SnapKV, designed for LLMs, struggle with VAR models due to their single-strategy compression. LOOK-M, using H2O’s eviction rule, suffers quality loss from aggressive merging in structural heads. HACK, with head-aware compression and merging, consistently outperforms the others, particularly at high compression.

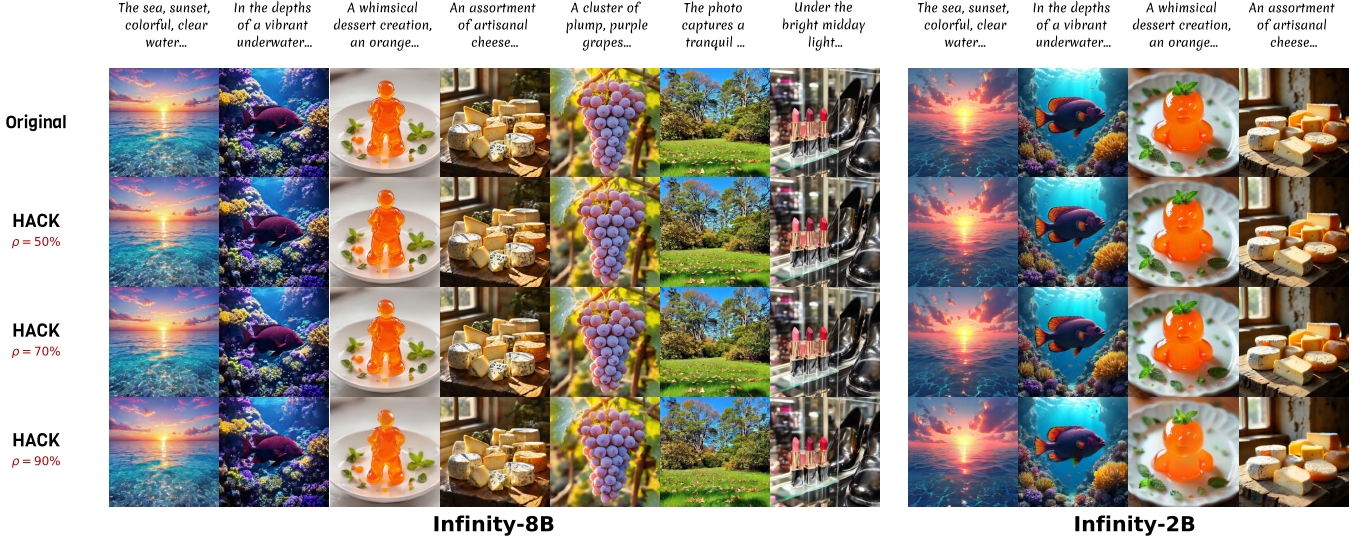


Figure 7: Qualitative comparison of images generated by HACK at different compression ratios on Infinity-8B and 2B models.

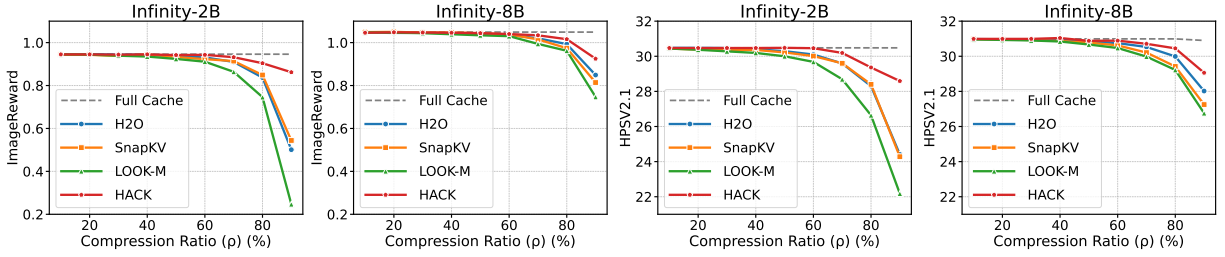


Figure 8: Performance comparison of different compression methods across varying compression ratios measured by ImageReward and HPSv2.1 on Infinity-2B and Infinity-8B.

Table 2: Quantitative comparison of class-conditional image generation on VAR-d30 at varying ρ values on ImageNet.

Method	ρ (%)	FID↓	sFID↓	IS↑	Precision↑	Recall↑
Full	0%	1.96	8.88	302.23	0.81	0.60
H2O [47]	30%	2.10	8.91	295.01	0.81	0.60
SnapKV [25]	30%	2.13	9.15	294.85	0.81	0.60
LOOK-M [41]	30%	3.32	10.40	255.36	0.76	0.61
HACK	30%	1.97	8.98	299.98	0.81	0.61
H2O [47]	50%	3.04	10.45	262.68	0.77	0.62
SnapKV [25]	50%	3.09	10.60	261.63	0.77	0.62
LOOK-M	50%	6.89	11.95	203.47	0.70	0.62
HACK	50%	2.06	9.29	293.60	0.80	0.61
H2O [47]	70%	8.81	12.59	182.84	0.68	0.62
SnapKV [25]	70%	7.31	12.54	196.62	0.70	0.62
LOOK-M [41]	70%	18.88	14.51	116.70	0.58	0.63
HACK	70%	2.78	10.54	268.69	0.78	0.62

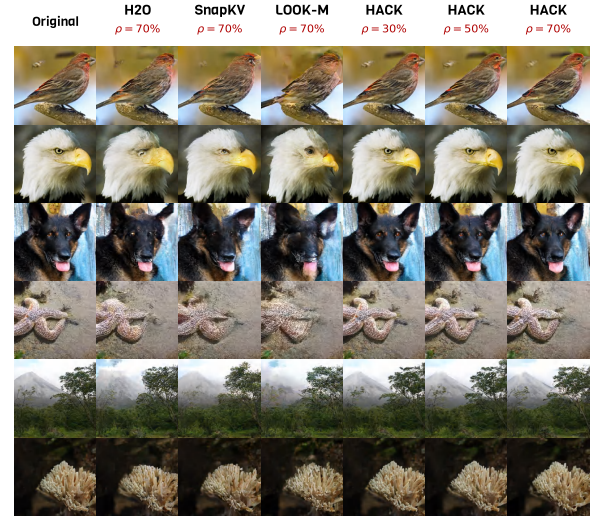


Figure 9: Qualitative comparison between original VAR-d30, HACK, and different compression methods. For more qualitative results, please refer to supplementary material.

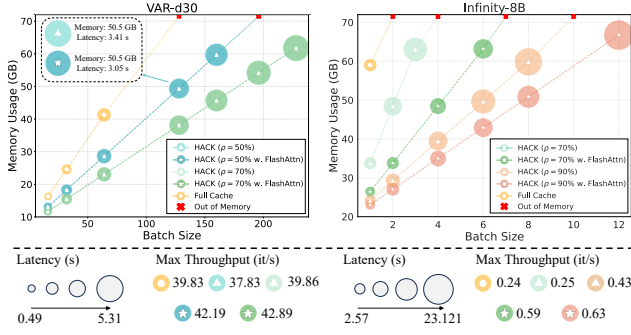


Figure 10: Memory and throughput comparison between full cache and HACK on VAR-d30 and Infinity-8B. The experiment is evaluated on NVIDIA H800 GPU.

Table 3: Component ablation on Infinity-2B (ImageReward \uparrow) and VAR-d30 (FID-50k \downarrow) across compression ratios ρ .

Asym. Budget	Pattern Comp.	Infinity-2B		VAR-d30	
		$\rho = 70\%$	$\rho = 90\%$	$\rho = 50\%$	$\rho = 70\%$
\times	\times	0.910	0.501	3.04	8.81
\checkmark	\times	0.914	0.578	2.19	5.40
\times	\checkmark	0.923	0.809	2.18	5.60
\checkmark	\checkmark	0.932	0.864	2.06	2.78

5.3 Class-Conditional Image Generation

We further evaluate the proposed HACK on class-conditional image generation using VAR-d30.

Quantitative Results. Table 2 shows HACK consistently outperforms baselines across compression ratios, with a larger margin at higher compression. For 256×256 VAR generation, the model’s sensitivity to compression is evident, as H2O, SnapKV, and LOOK-M see FID increases of 1.09, 1.13, and 4.93 at 50% compression, worsening at 70%. Merging strategies effective in LLMs perform poorly for VAR, with LOOK-M suffering most due to structural damage from repeated merging. HACK avoids this by merging only contextual heads at the final step, preserving semantics. It maintains stable quality with just a 0.13 FID increase at 50% compression and outperforms baselines at 70%, proving strong robustness.

Qualitative Results. Figure 9 shows that at 70% compression, baselines suffer severe distortions, while HACK consistently maintains high visual fidelity. This aligns with our quantitative results, highlighting HACK’s superior ability to preserve image quality under aggressive compression, thanks to its head-aware budget allocation and pattern-specific compression strategies.

5.4 Evaluation of Memory and Throughput

To validate HACK’s efficiency, we compared memory usage and inference throughput on VAR-d30 and Infinity-8B models. Figure 10 demonstrates that both models encounter memory constraints with full cache, resulting in OOM errors at batch sizes of 128 and 2, respectively. HACK effectively reduces KV cache storage and computational memory requirements by selectively pruning token caching

Table 4: Compression strategy ablation on Infinity-2B (ImageReward \uparrow) and VAR-d30 (FID-50k \downarrow) across varying ρ .

Strategy	Infinity-2B		VAR-d30	
	$\rho = 70\%$	$\rho = 90\%$	$\rho = 50\%$	$\rho = 70\%$
f_C w/o merge	0.931	0.860	2.09	2.82
f_S w/o init+k scales	0.908	0.787	2.86	5.75
Full $f_C + f_S$	0.932	0.862	2.06	2.78

Table 5: Query-subset selection strategy ablation on Infinity-2B/8B models evaluated by ImageReward \uparrow with $\rho = 90\%$.

Model	Random	Init	Recent	Uniform	Full
Infinity-2B	0.851	0.803	0.814	0.862	0.862
Infinity-8B	0.918	0.807	0.843	0.925	0.955

for each head. Our results show that HACK achieves memory reductions of 30.7% and 44.2% at compression ratios of 50% and 70% respectively for VAR-d30, and 42.8% and 58.9% at compression ratios of 70% and 90% for Infinity-8B. Notably, when integrated with FlashAttention in Infinity-8B, HACK further reduces memory usage while simultaneously increasing throughput by 162.5% (from 0.24 to 0.63) at compression ratios of 90% compared with full cache. These results conclusively demonstrate HACK’s efficiency and compatibility with existing optimization techniques, making it particularly well-suited for deployment in resource-constrained environments.

5.5 Ablation Study

Impact of Key Components. Table 3 examines HACK’s key components: asymmetric budget allocation and pattern-specific compression. Removing both results in significant performance drops, especially at higher compression ratios. Asymmetric budget allocation improves cache distribution, while pattern-specific compression enhances performance but lacks optimal budget distribution. The full HACK method, combining both, consistently achieves the best performance, demonstrating their complementary benefits.

Ablation Study on Compression Strategies. Table 4 evaluates our compression strategies for contextual (f_C) and structural (f_S) heads. Merging operations preserve semantic information for contextual heads while retaining initial and recent scale (init + k scales) tokens is critical for structural heads. These results confirm that each component tackles specific challenges in compressing VAR’s KV cache, with the overall approach achieving the best performance across models and compression settings.

Impact of Query Subset Selection. Table 5 evaluates the impact of different query selection strategies on compression performance in query-subset attention. We compare four strategies with a sampling size of $N = 32$: Random sampling, Initial-N (first N tokens), Recent-N (most recent N tokens), and Uniform sampling across all queries. Among them, Uniform sampling yields the performance closest to that of full attention, striking an optimal balance between computational efficiency and generation quality.

Due to space constraints, ablations on hyperparameter sensitivity and design components are deferred to the supplementary material.

6 Conclusion

We propose HACK, a training-free head-aware KV cache compression approach for VAR models. By efficiently identifying distinct structural and contextual attention head patterns, HACK allocates asymmetric cache budgets and applies specialized compression strategies optimized for each head type’s characteristics. HACK compresses each head type in an appropriate manner, balancing both strategy selection and budget allocation to preserve critical information. Extensive experiments on text-to-image and class-conditional generation models validate HACK’s effectiveness in achieving high compression ratios for KV cache while maintaining generation quality, demonstrating its practical utility for significantly reducing memory requirements in VAR models.

References

- [1] Josh Achiam, Steven Adler, Sandhini Agarwal, Lama Ahmad, Ilge Akkaya, Florencia Leoni Aleman, Diogo Almeida, Janko Altenschmidt, Sam Altman, Shyamal Anadkat, et al. 2023. Gpt-4 technical report. *arXiv preprint arXiv:2303.08774* (2023).
- [2] Anthropic. 2024. The Claude 3 Model Family: Opus, Sonnet, Haiku. https://www-cdn.anthropic.com/de8ba9b01c9ab7cbabf5c33b80b7bb6c18857627/Model_Card_Claude_3.pdf
- [3] Huayu Chen, Hang Su, Peize Sun, and Jun Zhu. 2024. Toward Guidance-Free AR Visual Generation via Condition Contrastive Alignment. *arXiv preprint arXiv:2410.09347* (2024).
- [4] Junsong Chen, Chongjian Ge, Enze Xie, Yue Wu, Lewei Yao, Xiaoze Ren, Zhongdao Wang, Ping Luo, Huchuan Lu, and Zhenguo Li. 2024. Pixart- σ : Weak-to-strong training of diffusion transformer for 4k text-to-image generation. In *European Conference on Computer Vision*. 74–91.
- [5] Yongwei Chen, Yushi Lan, Shangchen Zhou, Tengfei Wang, and Xingang Pan. 2025. SAR3D: Autoregressive 3D Object Generation and Understanding via Multi-scale 3D VQVAE. In *CVPR*.
- [6] Zigeng Chen, Xinyin Ma, Gongfan Fang, and Xinchao Wang. 2024. Collaborative Decoding Makes Visual Auto-Regressive Modeling Efficient. *arXiv preprint arXiv:2411.17787* (2024).
- [7] Zhiyuan Dang, Cheng Deng, Xu Yang, Kun Wei, and Heng Huang. 2021. Nearest neighbor matching for deep clustering. In *Proceedings of the IEEE/CVF conference on computer vision and pattern recognition*. 13693–13702.
- [8] Tri Dao. 2023. Flashattention-2: Faster attention with better parallelism and work partitioning. *arXiv preprint arXiv:2307.08691* (2023).
- [9] Jia Deng, Wei Dong, Richard Socher, Li-Jia Li, Kai Li, and Li Fei-Fei. 2009. Imagenet: A large-scale hierarchical image database. In *IEEE conference on computer vision and pattern recognition*. 248–255.
- [10] Abhimanyu Dubey, Abhinav Jauhri, Abhinav Pandey, Abhishek Kadian, Ahmad Al-Dahle, Aiesha Letman, Akhil Mathur, Alan Schelten, Amy Yang, Angela Fan, et al. 2024. The llama 3 herd of models. *arXiv preprint arXiv:2407.21783* (2024).
- [11] Patrick Esser, Sumith Kulal, Andreas Blattmann, Rahim Entezari, Jonas Müller, Harry Saini, Yam Levi, Dominik Lorenz, Axel Sauer, Frederic Boesel, et al. 2024. Scaling rectified flow transformers for high-resolution image synthesis. In *Forty-first international conference on machine learning*.
- [12] Patrick Esser, Robin Rombach, and Bjorn Ommer. 2021. Taming transformers for high-resolution image synthesis. In *Proceedings of the IEEE/CVF conference on computer vision and pattern recognition*. 12873–12883.
- [13] Yuan Feng, Junlin Lv, Yukun Cao, Xike Xie, and S Kevin Zhou. 2024. Ada-kv: Optimizing kv cache eviction by adaptive budget allocation for efficient llm inference. *arXiv preprint arXiv:2407.11550* (2024).
- [14] Yu Fu, Zefan Cai, Abedelkadir Asi, Wayne Xiong, Yue Dong, and Wen Xiao. 2024. Not all heads matter: A head-level KV cache compression method with integrated retrieval and reasoning. *arXiv preprint arXiv:2410.19258* (2024).
- [15] Jingnan Gao, Weizhe Liu, Weixuan Sun, Senbo Wang, Xibin Song, Taizhang Shang, Shenzhou Chen, Hongdong Li, Xiaokang Yang, Yichao Yan, et al. 2025. MARS: Mesh AutoRegressive Model for 3D Shape Detailization. *arXiv preprint arXiv:2502.11390* (2025).
- [16] Suyu Ge, Yunan Zhang, Liyuan Liu, Minjia Zhang, Jiawei Han, and Jianfeng Gao. 2023. Model tells you what to discard: Adaptive kv cache compression for llms. *arXiv preprint arXiv:2310.01801* (2023).
- [17] Dhruva Ghosh, Hannaneh Hajishirzi, and Ludwig Schmidt. 2023. Geneval: An object-focused framework for evaluating text-to-image alignment. *Advances in Neural Information Processing Systems* (2023), 52132–52152.
- [18] Jian Han, Jinlai Liu, Yi Jiang, Bin Yan, Yuqi Zhang, Zehuan Yuan, Bingyue Peng, and Xiaobing Liu. 2024. Infinity: Scaling bitwise autoregressive modeling for high-resolution image synthesis. *arXiv preprint arXiv:2412.04431* (2024).
- [19] Wanggui He, Siming Fu, Mushui Liu, Xierui Wang, Wenyi Xiao, Fangxun Shu, Yi Wang, Lei Zhang, Zhelun Yu, Haoyuan Li, et al. 2024. Mars: Mixture of auto-regressive models for fine-grained text-to-image synthesis. *arXiv preprint arXiv:2407.07614* (2024).
- [20] Yefei He, Luoming Zhang, Weijia Wu, Jing Liu, Hong Zhou, and Bohan Zhuang. 2024. ZipCache: Accurate and Efficient KV Cache Quantization with Salient Token Identification. *arXiv preprint arXiv:2405.14256* (2024).
- [21] Jonathan Ho, Ajay Jain, and Pieter Abbeel. 2020. Denoising diffusion probabilistic models. In *Advances in neural information processing systems*. 6840–6851.
- [22] Xiwei Hu, Rui Wang, Yixiao Fang, Bin Fu, Pei Cheng, and Gang Yu. 2024. Ella: Equip diffusion models with llm for enhanced semantic alignment. *arXiv preprint arXiv:2403.05135* (2024).
- [23] Hao Kang, Qingru Zhang, Souvik Kundu, Geonhwa Jeong, Zaoxing Liu, Tushar Krishna, and Tuo Zhao. 2024. Gear: An efficient kv cache compression recipe for near-lossless generative inference of llm. *arXiv preprint arXiv:2403.05527* (2024).
- [24] Tianhong Li, Yonglong Tian, He Li, Mingyang Deng, and Kaiming He. 2024. Autoregressive image generation without vector quantization. *Advances in Neural Information Processing Systems* 37 (2024), 56424–56445.
- [25] Yuhong Li, Yingbing Huang, Bowen Yang, Bharat Venkitesh, Acyr Locatelli, Hanchen Ye, Tianle Cai, Patrick Lewis, and Deming Chen. 2024. Snapkv: Llm knows what you are looking for before generation. *arXiv preprint arXiv:2404.14469* (2024).
- [26] Aixiu Liu, Bei Feng, Bing Xue, Bingxuan Wang, Bochao Wu, Chengda Lu, Chenggang Zhang, Chengqi Deng, Chenyu Zhang, Chong Ruan, et al. 2024. Deepseek-v3 technical report. *arXiv preprint arXiv:2412.19437* (2024).
- [27] Akide Liu, Jing Liu, Zizheng Pan, Yefei He, Gholamreza Haffari, and Bohan Zhuang. 2024. MiniCache: KV Cache Compression in Depth Dimension for Large Language Models. *arXiv preprint arXiv:2405.14366* (2024).
- [28] Zichang Liu, Aditya Desai, Fangshuo Liao, Weitao Wang, Victor Xie, Zhaozhao Xu, Anastasios Kyrillidis, and Anshumali Shrivastava. 2024. Scissorhands: Exploiting the persistence of importance hypothesis for llm kv cache compression at test time. *Advances in Neural Information Processing Systems* 36 (2024).
- [29] Zirui Liu, Jiayi Yuan, Hongye Jin, Shaochen Zhong, Zhaozhao Xu, Vladimir Braverman, Beidi Chen, and Xia Hu. 2024. Kivi: A tuning-free asymmetric 2bit quantization for kv cache. *arXiv preprint arXiv:2402.02750* (2024).
- [30] Matanel Oren, Michael Hassid, Yossi Adi, and Roy Schwartz. 2024. Transformers are multi-state rnns. *arXiv preprint arXiv:2401.06104* (2024).
- [31] William Peebles and Saining Xie. 2023. Scalable diffusion models with transformers. In *Proceedings of the IEEE/CVF international conference on computer vision*. 4195–4205.
- [32] Dustin Podell, Zion English, Kyle Lacey, Andreas Blattmann, Tim Dockhorn, Jonas Müller, Joe Penna, and Robin Rombach. 2023. Sdxl: Improving latent diffusion models for high-resolution image synthesis. *arXiv preprint arXiv:2307.01952* (2023).
- [33] Ziran Qin, Yuchen Cao, Mingbao Lin, Wen Hu, Shixuan Fan, Ke Cheng, Weiyao Lin, and Jianguo Li. [n. d.]. CAKE: Cascading and Adaptive KV Cache Eviction with Layer Preferences. In *The Thirteenth International Conference on Learning Representations*.
- [34] Sucheng Ren, Yaodong Yu, Nataniel Ruiz, Feng Wang, Alan Yuille, and Cihang Xie. 2024. M-VAR: Decoupled Scale-wise Autoregressive Modeling for High-Quality Image Generation. *arXiv preprint arXiv:2411.10433* (2024).
- [35] Siyu Ren and Kenny Q Zhu. 2024. On the efficacy of eviction policy for key-value constrained generative language model inference. *arXiv preprint arXiv:2402.06262* (2024).
- [36] Peize Sun, Yi Jiang, Shoufa Chen, Shilong Zhang, Bingyue Peng, Ping Luo, and Zehuan Yuan. 2024. Autoregressive model beats diffusion: Llama for scalable image generation. *arXiv preprint arXiv:2406.06525* (2024).
- [37] Keyu Tian, Yi Jiang, Zehuan Yuan, Bingyue Peng, and Liwei Wang. 2024. Visual autoregressive modeling: Scalable image generation via next-scale prediction. *Advances in neural information processing systems* 37 (2024), 84839–84865.
- [38] Aaron Van Den Oord, Oriol Vinyals, et al. 2017. Neural discrete representation learning. *Advances in neural information processing systems* 30 (2017).
- [39] Anton Voronov, Denis Kuznedelev, Mikhail Khoroshikh, Valentin Khrulkov, and Dmitry Baranchuk. 2024. Switti: Designing Scale-Wise Transformers for Text-to-Image Synthesis. *arXiv preprint arXiv:2412.01819*.
- [40] Zhongwei Wan, Xinjian Wu, Yu Zhang, Yi Xin, Chaofan Tao, Zhihong Zhu, Xin Wang, Siqi Luo, Jing Xiong, and Mi Zhang. 2024. D2O: Dynamic Discriminative Operations for Efficient Generative Inference of Large Language Models. *arXiv preprint arXiv:2406.13035* (2024).
- [41] Zhongwei Wan, Ziang Wu, Che Liu, Jinfa Huang, Zhihong Zhu, Peng Jin, Longyue Wang, and Li Yuan. 2024. Look-m: Look-once optimization in kv cache for efficient multimodal long-context inference. *arXiv preprint arXiv:2406.18139* (2024).
- [42] Xiaoshi Wu, Yiming Hao, Keqiang Sun, Yixiong Chen, Feng Zhu, Rui Zhao, and Hongsheng Li. 2023. Human preference score v2: A solid benchmark for evaluating human preferences of text-to-image synthesis. *arXiv preprint arXiv:2306.09341* (2023).

- [43] Jiazheng Xu, Xiao Liu, Yuchen Wu, Yuxuan Tong, Qinkai Li, Ming Ding, Jie Tang, and Yuxiao Dong. 2023. Imagereward: Learning and evaluating human preferences for text-to-image generation. *Advances in Neural Information Processing Systems* (2023), 15903–15935.
- [44] Dongjie Yang, XiaoDong Han, Yan Gao, Yao Hu, Shilin Zhang, and Hai Zhao. 2024. PyramidInfer: Pyramid KV Cache Compression for High-throughput LLM Inference. *arXiv preprint arXiv:2405.12532* (2024).
- [45] Yuxuan Yue, Zhihang Yuan, Haojie Duanmu, Sifan Zhou, Jianlong Wu, and Liqiang Nie. 2024. Wkvquant: Quantizing weight and key/value cache for large language models gains more. *arXiv preprint arXiv:2402.12065* (2024).
- [46] Yuxin Zhang, Yuxuan Du, Gen Luo, Yunshan Zhong, Zhenyu Zhang, Shiwei Liu, and Rongrong Ji. 2024. Cam: Cache merging for memory-efficient llms inference. In *Forty-first International Conference on Machine Learning*.
- [47] Zhenyu Zhang, Ying Sheng, Tianyi Zhou, Tianlong Chen, Lianmin Zheng, Ruisi Cai, Zhao Song, Yuandong Tian, Christopher Ré, Clark Barrett, et al. 2024. H2o: Heavy-hitter oracle for efficient generative inference of large language models. *Advances in Neural Information Processing Systems* 36 (2024).
- [48] Xianwei Zhuang, Yuxin Xie, Yufan Deng, Liming Liang, Jinghan Ru, Yuguo Yin, and Yuexian Zou. 2025. VARGPT: Unified Understanding and Generation in a Visual Autoregressive Multimodal Large Language Model. *arXiv preprint arXiv:2501.12327* (2025).

A Implementation Details

In our implementation of HACK, we perform offline head classification by randomly sampling prompts from ImageReward [43] for Infinity [18] and class labels from ImageNet1K [9] for VAR [37]. Given the stability of attention head patterns across different samples, we only use a sampling size of $N_s = 50$ as it is sufficient for reliable classification. We further analyze how the sampling size N_s affects head classification stability in Appendix C.2. The contextual head ratio α is set to 0.1, 0.3, and 0.35 for Infinity-2B, Infinity-8B, and VAR-d30, respectively, based on the empirical distribution of attention variance scores. For asymmetric budget allocation, we tune the λ parameter according to the compression ratio. In Infinity models, λ gradually decreases from 0.3 to 0.05 as the compression ratio reduces from 90% to 10%, ensuring more budget is reserved for structural heads under tighter memory constraints. For VAR-d30, we fix $\lambda = 0.1$ across all settings, as it consistently yields a good balance between memory efficiency and generation quality. For token eviction, we set $N = 32$ in query-subset attention for both Infinity and VAR models, based on our ablation results, which demonstrate that this setting closely approximates full attention while significantly improving efficiency.

B Compatibility and Comparison with Collaborative Decoding.

Recent work CoDe [6] explores an orthogonal direction to KV cache compression by leveraging collaborative decoding strategy to improve the inference efficiency of VAR models. CoDe employs a dual-model strategy: a large model (drafter) generates early-scale token maps focusing on low-frequency structure, while a smaller model (refiner) handles late-scale token maps, refining high-frequency details. We compare HACK against CoDe under its optimal setup, where the large model drafts the first 9 scales and the small model refines the last one, reducing peak KV cache memory by approximately 36.65%. To assess compatibility, we further apply HACK on top of CoDe, compressing an additional 30% of KV cache beyond CoDe’s reduction. Experiments are conducted on VAR-d30 using both CoDe’s training-free and fine-tuned settings, with default generation hyperparameters. As shown in Table 6, HACK alone surpasses CoDe in generation quality even under higher compression. Moreover, integrating HACK with CoDe achieves further KV cache savings without noticeable FID degradation. Unlike CoDe, which requires model specialization and fine-tuning, HACK is training-free and model-agnostic, offering a plug-and-play enhancement. These results highlight the practicality of integrating HACK into collaborative decoding frameworks to improve memory efficiency without additional complexity.

C Additional Ablation Study

C.1 Sensitivity Study on Hyperparameters

HACK involves two key hyperparameters: the contextual head ratio α , which controls the proportion of attention heads classified as contextual, and the budget weight λ , which determines the relative allocation of compression budget between contextual and structural heads. We evaluate the sensitivity of these hyperparameters on VAR-d30. The results are summarized in Table 7 and Table 8. As

Table 6: Compatibility and comparison with collaborative decoding. We evaluate both training-free (TF) and fine-tuned (FT) variants of CoDe, with and without the integration of HACK on VAR-d30.

Method	$\rho(\%)$	FID↓	sFID↓	IS↑	Precision↑	Recall↑
CoDe (TF)	37.6%	2.15	9.81	288.52	0.80	0.60
CoDe (FT)	37.6%	2.09	9.97	283.29	0.79	0.62
HACK	50%	2.06	9.29	293.60	0.80	0.61
CoDe (TF) w. HACK	56.4%	2.13	9.98	284.46	0.80	0.61
CoDe (FT) w. HACK	56.4%	2.09	10.04	281.93	0.79	0.62

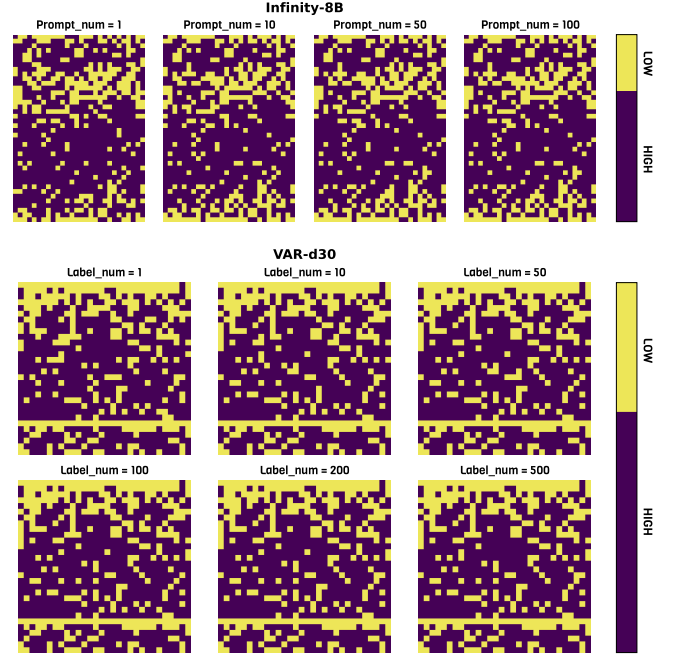
Table 7: Sensitivity study on α . We vary α and $\lambda = 0.1$, with different compression ratios ρ .

α	$\rho(\%)$	FID↓	sFID↓	IS↑	Precision↑	Recall↑
0.20	30%	1.98	9.00	300.25	0.81	0.61
0.30	30%	1.98	9.02	300.97	0.81	0.61
0.35	30%	1.97	8.98	299.98	0.81	0.61
0.40	30%	1.98	9.12	298.89	0.81	0.61
0.50	30%	2.06	9.32	292.75	0.80	0.61
0.20	50%	2.08	9.34	292.70	0.80	0.61
0.30	50%	2.07	9.30	293.2	0.80	0.61
0.35	50%	2.06	9.29	293.60	0.80	0.61
0.40	50%	2.10	9.45	291.28	0.80	0.61
0.50	50%	2.23	9.51	283.31	0.79	0.61
0.20	70%	4.46	10.87	235.94	0.74	0.62
0.30	70%	3.01	10.86	261.24	0.77	0.62
0.35	70%	2.78	10.54	268.69	0.78	0.62
0.40	70%	2.79	10.68	268.89	0.78	0.62
0.50	70%	2.93	10.56	263.32	0.78	0.62

shown in Table 7, appropriately tuning α can improve the performance of the compressed model. Moderate values (e.g., $\alpha = 0.35$) yield better generation quality, as they ensure sufficient budget is preserved for structural heads, which are critical for maintaining geometric consistency. Too low values under-utilize contextual compression opportunities, while too high values may misclassify structural heads and harm fidelity. In contrast, λ is a more sensitive parameter, as shown in Table 8. Increasing λ allocates more budget to contextual heads, resulting in a consistent performance drop. This is because contextual heads require minimal memory to retain global semantics, and over-allocating memory to them reduces the budget available for structural heads—leading to degradation in spatial fidelity and overall image quality. Our results suggest that a lower value of λ enables a more effective budget allocation that prioritizes structural heads, which is crucial for maintaining spatial integrity in VAR models.

Table 8: Sensitivity study on λ . We vary λ and $\alpha = 0.35$, with compression ratio $\rho = 70\%$.

λ	FID↓	sFID↓	IS↑	Precision↑	Recall↑
0.10	1.97	8.98	299.98	0.81	0.61
0.15	3.99	10.75	245.35	0.75	0.62
0.20	4.31	10.77	239.09	0.74	0.62
0.30	5.59	11.01	220.96	0.72	0.63
0.40	7.31	11.25	199.55	0.69	0.63

**Figure 11: Head classification results of Infinity-8B and VAR models with varying N_s prompts/labels. Yellow indicates Contextual Heads (low variance); purple indicates Structural Heads (high variance).**

C.2 Impact of Samples' Size on Head Classification

To evaluate the effect of the number N_s of prompts or class labels on the offline classification of attention head patterns, we conduct experiments across varying N_s values. As shown in Figure 11, both Infinity-8B and VAR-d30 exhibit highly stable head classification results, regardless of the number of prompts (from 1 to 100) or class labels (from 1 to 500). This observation supports our core finding: the functional roles of attention heads remain largely invariant across sample sizes, suggesting a strong inductive prior in head behavior. We select $N_s = 50$ as it provides sufficiently clear head-wise separability while maintaining minimal labeling cost.

Table 9: Impact of sampling size N on query-subset attention. The experiments are conducted on Infinity-2B using ImageReward (\uparrow).

$\rho(\%)$	$N = 4$	$N = 8$	$N = 16$	$N = 32$	Full
70%	0.923	0.928	0.929	0.932	0.931
90%	0.800	0.856	0.843	0.862	0.862

Table 10: Influence of merge steps for contextual head compression strategy f_C . The experiments are conducted on VAR-d30 using Imagenet1K with $\rho = 70\%$.

Method	Merge Steps	FID \downarrow	sFID \downarrow	IS \uparrow	Precision \uparrow	Recall \uparrow
w/o merge	0	2.82	10.59	266.84	0.78	0.62
Start step = 10	1	2.78	10.54	268.69	0.78	0.62
Start step = 9	2	2.78	10.50	268.40	0.78	0.61
Start step = 8	3	2.78	10.51	268.39	0.79	0.62

C.3 Impact of Sampling Size on Query-subset Attention

Table 9 presents the impact of sampling size N on the effectiveness of query-subset attention. As N increases, the compressed model demonstrates progressively improved performance, approaching that of full attention. This is because a larger query subset allows for more accurate estimation of token importance. Remarkably, when $N = 32$, the model achieves performance nearly equivalent to the full attention baseline, striking a favorable balance between accuracy and efficiency. We adopt $N = 32$ in our main experiments.

C.4 Impact of merge operation steps for f_C

We study the effect of different merge operation schedules in the contextual head compression strategy f_C . As shown in Table 10, applying the merge operation only at the final generation step leads to the most notable improvement in generation quality, significantly reducing FID and enhancing Inception score. However, increasing the number of merge steps to earlier stages (e.g., steps 9 and 8) offers limited additional benefit and, in some cases, slightly degrades performance. This suggests that contextual merging is most effective when applied at the highest-resolution stage, where the model attends to fine-grained visual details. Earlier merges may interfere with the coarse-to-fine progression and introduce unnecessary perturbations. Based on these findings, we adopt a single-step merge at the final scale as the default configuration for f_C in our experiments.

D Additional Qualitative Results

In this section, we provide additional qualitative results on Infinity-2B/8B and VAR-d30 models. For images generated by Infinity models, we use prompts sampled from DPG [22], which offer diverse and high-level scene descriptions. For VAR-d30, we sample class labels from ImageNet-1K [9]. Figures 12 and 13 present more generation results under different compression ratios ρ on Infinity-2B and Infinity-8B, respectively. Across various sparsity levels, HACK consistently maintains high generation quality, even under extreme

compression ratios (e.g., 90%). The model preserves structure, layout, and semantic consistency despite significant memory reduction. Figure 14 and Figure 15 further compare HACK with baseline methods (H2O [47], SnapKV [25], and LOOK-M [41]) on both Infinity-2B and VAR-d30 across multiple compression ratios ρ . At lower compression levels, all methods perform reasonably well due to token redundancy in VAR models. However, as the compression ratio increases, baseline methods struggle to retain visual fidelity due to improper compression of structural heads, resulting in the loss of critical scene information. In contrast, HACK benefits from its head-aware design, selectively compressing contextual heads while preserving structurally important ones. As a result, even at high compression levels, HACK consistently retains scene layout, object integrity, and alignment with the original outputs, demonstrating both effectiveness and robustness.

E Additional Analysis for Attention Patterns

To complement our main analysis, we provide additional attention visualizations in VAR-based models. As shown in Figure 16, both Infinity-8B and VAR-d30 consistently exhibit two distinct types of attention heads: *structural heads*, which display diagonal or band-like patterns capturing local spatial dependencies, and *contextual heads*, which show vertical patterns focusing on global token relevance irrespective of spatial position. Furthermore, in Figure 17, we visualize the same head across multiple samples and observe that the pattern type remains stable regardless of the input. This reaffirms our observation that the distinction between structural and contextual heads is an intrinsic property of the model, not dependent on specific prompts or class labels. Therefore, the proposed offline head classification method is reliable and data-efficient, supporting our head-aware KV cache compression design.

These qualitative results further emphasize the need for head-aware compression strategies, as single-pattern assumptions fail to accommodate the diverse roles of attention heads in VAR models.

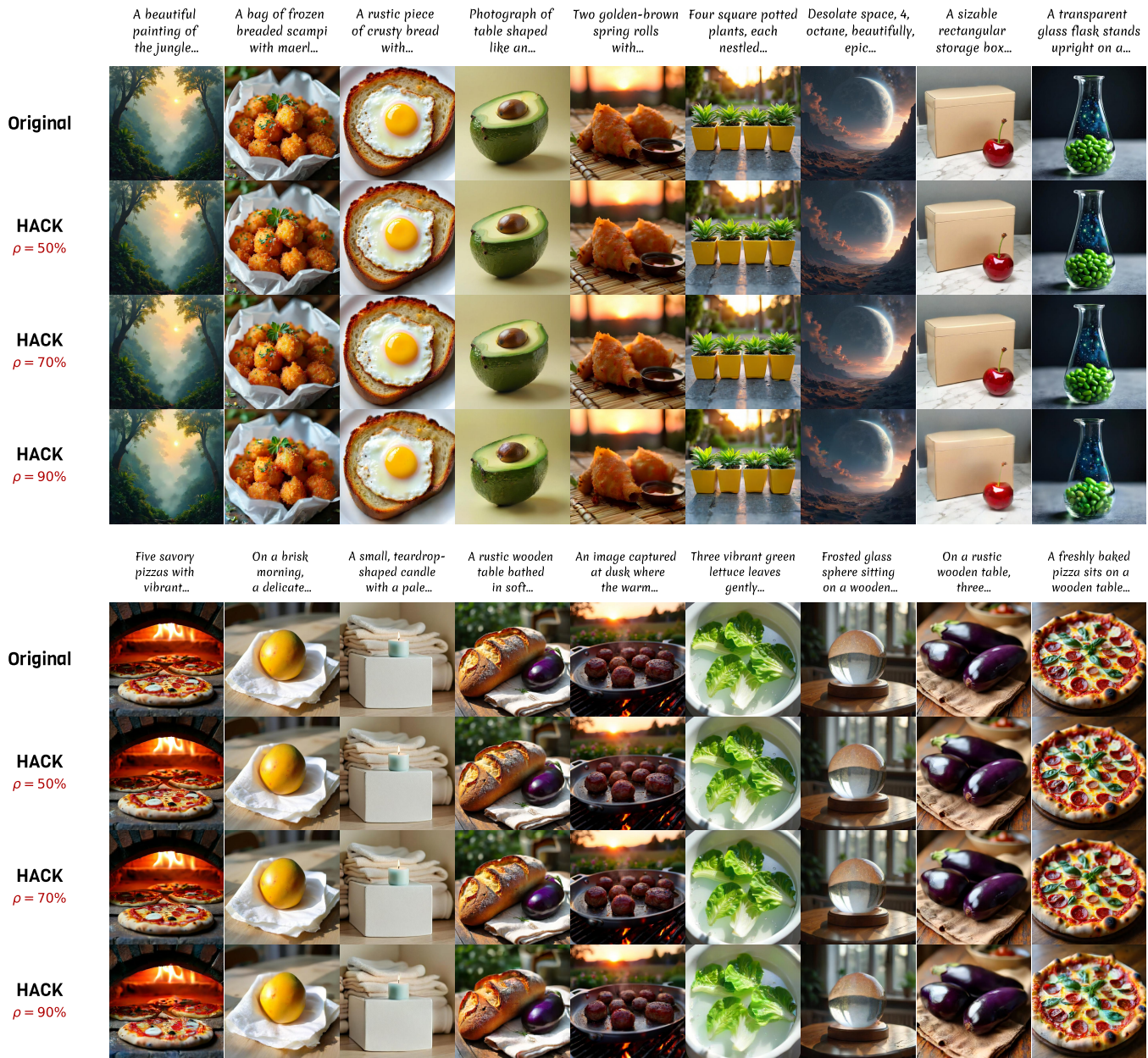


Figure 12: Qualitative comparison of images generated by Infinity-2B under different compression ratios using HACK.

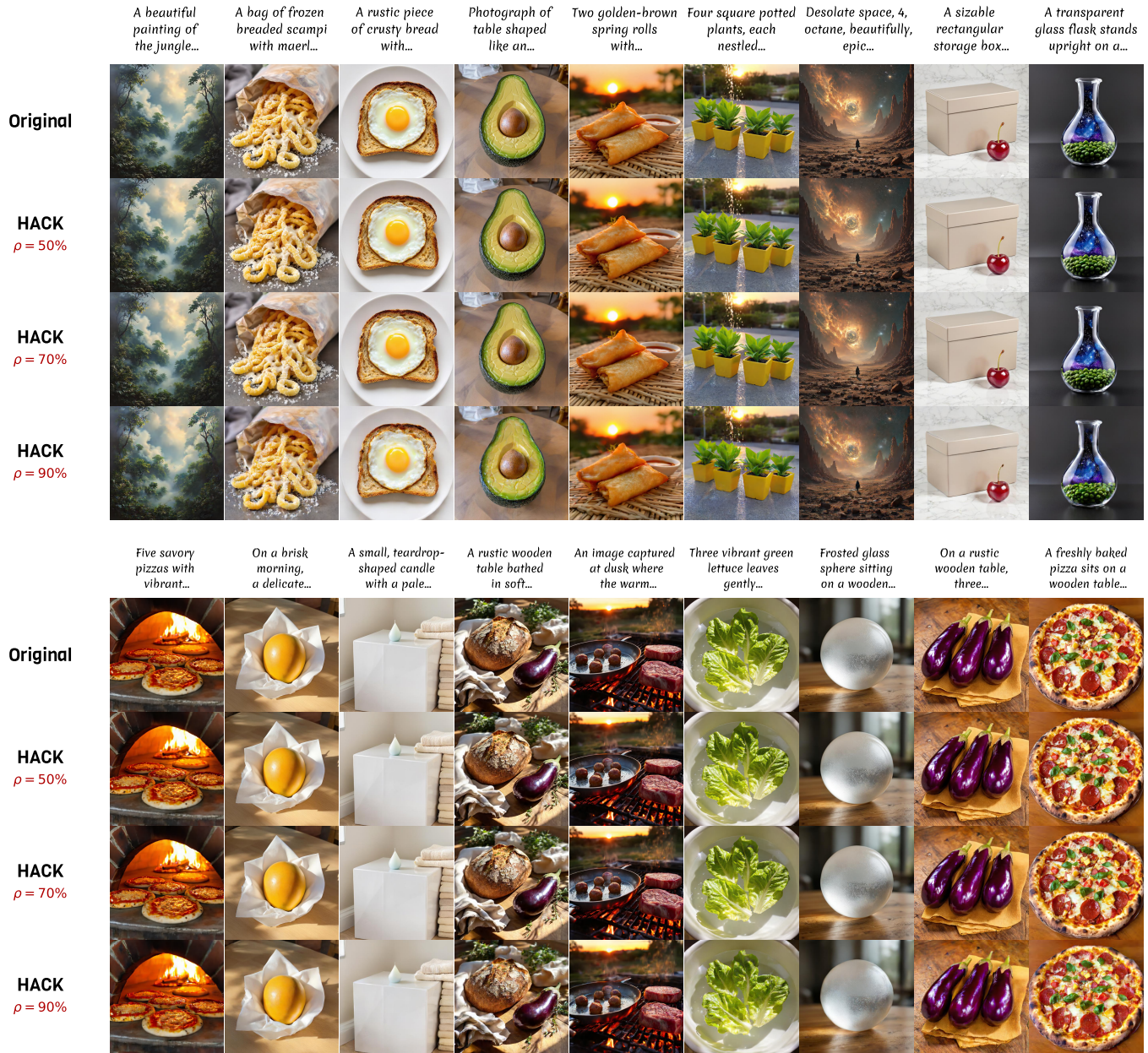


Figure 13: Qualitative comparison of images generated by Infinity-8B under different compression ratios using HACK.



Figure 14: Comparison between HACK and baseline methods on Infinity-2B under varying compression ratios.



Figure 15: Comparison between HACK and baseline methods on VAR-d30 under varying compression ratios.



Figure 16: Additional visualizations of structural and contextual heads in VAR-d30 and Infinity-8B.



Figure 17: Additional visualizations of structural and contextual heads across different input samples in VAR-d30 and Infinity-8B.